Stopping Cross Section of Low Atomic Number Materials

for He$^+$, 65-180 keV

R. Dale Moorhead

National Aeronautics and Space Administration

Ames Research Center, Moffett Field, California

ABSTRACT

29380

Stopping cross sections were measured for H_1^+ in carbon
and for He$^+$ in carbon, aluminum, and chromium over the energy
range of 65 to 180 keV. Layers of the stopping materials were
evaporated in vacuo onto a gold-plated quartz crystal and their
areal densities were computed from the shift in the resonant
frequency of the crystal. The energy lost by the ions in the
stopping material was determined by measuring the energy of
the scattered ions. Experimental results show a divergence
from available theory above 80 keV.

author

INTRODUCTION

There are many areas of physics where a knowledge of stopping cross sections is important. In particular, they aid in the determination of the screened-interaction potential which is fundamental to the theoretical understanding of radiation damage and sputtering phenomena. Accurate stopping cross sections are also required for the proper interpretation of various nuclear reaction cross section measurements. Finally, recent calculations[1] related to the differential energy loss suffered by low energy ions have reached the point where detailed comparison with experiment is desirable.

The present experiments were undertaken to provide absolute stopping cross section measurements for selected ion-medium combinations in the range of ion energy from 65 to 180 keV where data are relatively sparse or nonexistent.
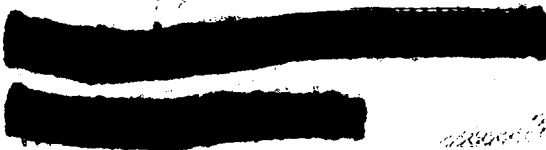
EXPERIMENTAL PROCEDURE

The stopping cross section per atom, S_O, of a substance for a penetrating particle is defined by the equation

$$S_O = -(1/N)(dE/dR),$$

where N is the number of stopping atoms per unit volume of the substance and dE is the energy lost by the particle in traversing a distance dR through the stopping substance.

To measure stopping cross sections directly, two quantities must be determined: $N\Delta R$, which is related to the mass per unit area of the stopping

medium parallel to the path of the penetrating ions; and ΔE, the amount of energy lost by the ions as they pass through this amount of material. In this experiment, ΔE was measured with a high resolution (0.1%) electrostatic energy analyzer operated symmetrically. The quantity $N\Delta R$ was determined by noting the change in the fundamental frequency of a piezo-electric quartz crystal as a layer of the stopping material was evaporated onto one of its faces.

Apparatus

Positive ion beams were generated and mass separated in a 50 to 200 keV Cockcroft-Walton accelerator equipped with a Von Ardenne ion source and a 19.5° magnetic analyzer. The ions were collimated onto the target through a series of apertures that reduced the beam diameter to 1.27 mm (Fig. 1) and the current to about 0.2 μA. The target was located at the first focus of the 117° energy analyzer. Particles scattered by the target at an angle of 160° entered the analyzer through slit s_1 which was biased to -300 V to suppress secondary electrons. Ions selected by the analyzer were detected by a NaI-photomultiplier combination behind exit slit s_2 located at the second focus.

The pressure in the target chamber was maintained at less than 5×10^{-6} mm Hg with cryogenically baffled diffusion pumps.

Targets

Targets were prepared on commercially available A.T. cut crystals that had a natural frequency of 7.5 Mc/sec. The crystals were quartz disks of

of 1.34-cm diameter with a matte finish. Gold electrodes, approximately
equal in thickness, were evaporated onto each face of the crystals so as
to cover both surfaces completely.

The stopping material was evaporated onto one side of the gold-plated
crystal inside the test chamber (see Fig. 1) and all subsequent measure-
ments were made without exposing the test material to the atmosphere.
The areal density of the evaporated layer was monitored by continuously
measuring the crystal frequency during evaporation. The densities used
ranged from 4×10^{-6} to 13×10^{-6} g/cm^2, corresponding to frequency shifts of
500 to 1600 cps. Most of the targets were 8×10^{-6} g/cm^2 ($\Delta f = 1000$ cps).

The areal density of the stopping layer, φ, was computed from the
formula[2]

$$\varphi = (\Delta f K/f^2), \; g/cm^2.$$

In this equation Δf represents the frequency change, K is a constant of
the crystal, in this case 4.425×10^5 cps g/cm^2, and f is the frequency of
the crystal just prior to evaporation and includes the effects of the gold
electrodes and crystal holder.

The target was mounted so it could be rotated 180° around an axis
perpendicular to the beam. Thus, both faces could be exposed to the inci-
dent ions. Transverse motion along this axis was also possible. In addi-
tion, the target could be rotated slowly around an axis normal to its
surface. With this latter axis passing through the surface at a point
offset from the beam, rotation resulted in scanning an annular region of
the target during a measurement. This scanning was found to be necessary

in order to avoid errors associated with changes in the target surface caused by prolonged ion bombardment. Furthermore, it provided a means of checking the uniformity of the stopping layer.

Energy Measurements

The electrostatic analyzer had a mean radius of 11.375 in. and a plate separation of 0.100 in. Voltage to the plates was supplied by two direct reading precision power supplies. For a potential difference, ΔV_a, between the plates, the energy of acceptance, E_a, of the analyzer was computed from the equation

$$E_a = (L/2l) \Delta V_a q$$

where L is the mean radius, l is the plate separation, and q is the charge on the ion.

The ion current to the target was metered through a current integrator. The number of scattered ions reaching the analyzer detector for a fixed integrated current on the target was recorded as a function of the acceptance energy of the analyzer. Typical energy distributions of the scattered beam are shown in Fig. 2. Curve (b) is for ions scattered from the clean gold face of the target, while curve (a) is for ions which have gone through the stopping substance and rebounded from the underlying gold electrode. The effective energy of the ions was taken as that corresponding to half the maximum accumulated counts.[3] The energy measured from curve (b), when corrected to account for the recoil energy of the gold atoms, is equal to the energy of the incident ions. The operating voltage

Fig.

of the accelerator, known to within about 5%, thus served as a secondary measure of ion energy.

Data Reduction

The events that change the energy of the ions at the target are diagrammed in Fig. 3. The energy of the ions from the accelerator is E_1, and their energy into the analyzer is E_4. The energy transferred to the stopping material is $E_1 - E_2$ in a thickness ΔR_1, and $E_3 - E_4$ in a thickness ΔR_2. The quantity $E_2 - E_3$ is the energy lost in the recoil process from the gold substratum; this can be estimated on the assumption of an elastic collision:

$$E_2 - E_3 = (1 - \rho)E_2 \tag{1}$$

where ρ, the well-known elastic scattering factor, is given by,

$$\rho = \frac{M_2{}^2 - M_1{}^2(1 - 2\cos^2\alpha) \pm 2M_1 \cos\alpha(M_2{}^2 - M_1{}^2 \sin^2\alpha)^{1/2}}{(M_1 + M_2)^2} .$$

In this notation M_1 is the mass of the projectile particle, M_2 the mass of the target atom (gold in this experiment), and α is the scattering angle ($160°$ for ions entering the analyzer). Values of ρ were 0.92 for He^+ and 0.98 for $H_1{}^+$.

The quantity $E_1 - E_4$ can be written in terms of the foregoing individual loss processes as follows:

$$E_1 - E_4 = (E_3 - E_4) + (E_2 - E_3) + (E_1 - E_2). \tag{2}$$

We may also write:

$$dE_1/dR_1 \approx \Delta E_1/\Delta R_1 = (E_1 - E_2)/\Delta R_1 \; ; \qquad dE_2/dR_2 \approx \Delta E_2/\Delta R_2 = (E_3 - E_4)/\Delta R_2 . \quad (3)$$

Combining Eqs. (1), (2), and (3) gives:

$$\rho E_1 - E_4 = (dE_2/dR_2)\Delta R_2 + \rho(dE_1/dR_1)(\Delta R_1). \qquad (4)$$

Two new terms, E and dE/dR, can now be approximated from the expressions:

$$dE_1/dR_1 = (dE/dR) + [(\partial/\partial E)(dE/dR)](E_1 - E),$$

$$dE_2/dR_2 = (dE/dR) - [(\partial/\partial E)(dE/dR)](E - E_4),$$

where the new quantities are the coordinates of a point Q on the represent-
ative curve shown in Fig. 4. Substituting these expressions into Eq. (4),
one obtains:

$$\rho E_1 - E_4 = (\Delta R_2 + \rho\Delta R_1)(dE/dR) + [(\partial/\partial E)(dE/dR)][\rho\Delta R_1(E_1 - E) - \Delta R_2(E - E_4)].$$

If a value of E is chosen such that the second term on the right side of
the above equation can be equated to zero, two expressions are obtained that
define E and dE/dR in terms of known or measured quantities:

$$E = (\rho g E_1 + E_4)/(1 + \rho g), \qquad (5a)$$

$$dE/dR = (\rho E_1 - E_4)/[\Delta R_2(1 + \rho g)], \qquad (5b)$$

where $g = \Delta R_1/\Delta R_2$. Again Fig. 3 shows that

$$\Delta R_i = \Delta R/\cos \theta_i ,$$

where θ_i corresponds to θ_1 and θ_2, the angles between the target normal
and the trajectories of the incident and exit ions. ΔR_i corresponds to
ΔR_1 and ΔR_2, respectively, and ΔR is the target thickness. It was the
usual practice to set the angles equal to each other so g equalled one.

The observed stopping cross section at energy E is then,

$$S_O(E) = (\Delta E/N\Delta R)\cos \theta_2 \qquad\qquad (6)$$

with ΔE equal to $(\rho E_1 - E_4)/(1 + \rho g)$.

RESULTS

Cross sections computed from Eqs. (5a) and (6) are shown in Figs. 5-8.
Smooth curves were visually fitted to the experimental points, and values
from these curves are listed in Table I at various energy intervals. The
probable error in these data is calculated to be approximately 3% from
estimated errors in $N\Delta R$ and ΔE (Eq. (6)) of 1.5% and 2.5%, respectively.
The internal consistency of these measurements agrees with the 3% probable
error. Individual data points deviate from their respective curves by less
than 3%, and the average deviation from each curve is less than 1%. The
gradual change in the slopes of the curves tends to make any errors attrib-
utable to the approximate nature of Eq. (6) small compared to those
mentioned above.

Data recently published by Ormrod and Duckworth[4] are compared with
some of the results of this experiment in Figs. 5 and 6. The agreement
between the two sets of data is particularly good for protons on carbon
(Fig. 5), where the two sets of data connect smoothly. Comparable data for
helium on carbon (Fig. 6) differ by about 3.2%. Also shown in Fig. 5 is
proton-carbon data published by Reynolds, et al.[5] They obtained their
data by applying Bragg's rule to observed cross sections of various
hydrocarbon gases.

DISCUSSION

Throughout the greater part of their range, the predominant mechanism by which ions lose energy is inelastic electronic collisions. An expression for the electronic stopping cross section per atom, S_e, appropriate to the energy range of this experiment was derived theoretically by Lindhard and Scharff[1] and can be written in terms of the energy of the penetrating ions, E, as

$$S_e = \xi_e Z_1^{2/3}(8\pi e^2 a_0)[Z_1 Z_2 / (Z_1^{2/3} + Z_2^{2/3})^{3/2}](E/E_0)^{1/2}, \qquad (7)$$

where E_0 is the kinetic energy of the ions when their speed is $v_1 = v_0 Z_1^{2/3}$; v_0 is the velocity of the electron in the first Bohr orbit in hydrogen; Z and M (Eq. (8)) represent atomic numbers and mass; and a_0 is the Bohr radius. The subscripts 1 and 2 refer to the penetrating ions and the stopping medium, respectively. The factor ξ_e is thought to have a value between 1 and 2 and possibly equal to $Z_1^{1/6}$. Equation (7) is supposed to be valid for $E < E_0$. For He^+, $E_0 \cong 250$ keV.

When the ions approach the terminal portion of their range, elastic collisions that impart energy to the nuclei of the stopping medium become important. Bohr[6] has found that when these collisions are predominantly of the Rutherford type, the nuclear stopping cross section per atom, S_n, can be expressed approximately as

$$S_n \cong 2\pi (M_1/M_2) e^4 (Z_1^2 Z_2^2/E) \ln(2\epsilon), \qquad (8)$$

where

$$\epsilon = E\{0.8853 a_0 / [Z_1 Z_2 (Z_1^{2/3} + Z_2)^{1/2} e^2\}[M_2/(M_1 + M_2)].$$

A correction to Eq. (8) (small for the ion velocities of this experiment) to account for screening effects on nuclear collisions has been computed by Lindhard and Thomsen.[7]

The total stopping cross section per atom is, of course, the sum of the separate components $S_e + S_n$.

The theoretical curves plotted in Figs. 6, 7, and 8 were computed from Eq. (7) plus a small contribution ($< 2\%$ of S_0) from Eq. (8) corrected for screening effects.[7] The parameter ξ_e was chosen in each case for agreement with experiment at a low value of energy (81 keV) where the theory should be most valid. The values of ξ_e so determined are listed below.

Ion	Stopping material	Z_2	ξ_e
He^+	C	6	1.23
He^+	Al	13	1.59
He^+	Cr	24	2.03

Since the largest contribution to the total stopping cross section in the energy range covered by this experiment is from the electronic component, it is appropriate at this point to mention the limitations of Eq. (7). In Ref. 1, Lindhard and Scharff state: "The dependence of S on Z_1 and Z_2 is an expedient to get sample estimates." Elsewhere,[8] Lindhard has been quoted as saying: "It should be emphasized that Eq. (7) is approximate in more than one sense. The constant ($\xi_e \cong Z_1^{1/6}$) is based on Thomas-Fermi arguments, and it is to be expected that fluctuations around this constant can occur, especially for $Z_1 \leq 10$. Moreover, a precise proportionality to v (i.e., $E^{1/2}$) will not be correct over the whole of the velocity region $v < v_1$ ($E < E_0$)."

Within the confines of these limitations, we find essential agreement between our experimental results and theoretical predictions. In Figs. 6, 7, and 8, it is seen that the agreement is limited to the low energy region as expected. Moreover, this agreement is evidence of a velocity dependence on S_e in this region, when a small correction for nuclear effects is included in the total measured cross section. We note, however, that the range of agreement for a given ion varies with the stopping material. Agreement stops at 80 keV for He^+ on carbon and 130 keV for He^+ on aluminum or on chromium.

Although the values of ξ_e listed above lie between 1 and 2 within experimental scatter, ξ_e is definitely dependent on the stopping material, i.e., Z_2, and the increasing trend found here would suggest values of $\xi_e > 2$ for larger values of Z_2. This variation of ξ_e with Z_2 may be due to the "simplified" Z dependence assumed for S_e mentioned above. If this should be the case, the simple relationship between ξ_e and Z_2 found from this work may be of interest. From the three values obtained in this experiment, we find $\xi_e \propto Z_2^{0.354}$. We hasten to point out that this result may be entirely fortuitous or may be related to the fact that the atomic numbers of the stopping materials are nearly in the ratio 1:2:4 (a periodic variation of ξ_e with Z_1 was found by Ormrod, et al.).[4] In any event, we wish to emphasize that this result cannot be considered as anything more than an interesting observation at this time.

SUMMARY

Absolute measurements of the total stopping cross section have been made for H_1^+ in carbon and for He^+ in carbon, aluminum, and chromium for energies ranging from 65 to 180 keV. The results are listed in Table I.

The results of the He^+ measurements have been used to compare the dependence of Eq. (7) on the parameters E and Z_2 with experiment. In the low energy region the implicit velocity dependence of Eq. (7) is in essential agreement with experimental findings. However, the experimental results indicate that the Z_2 dependence of Eq. (7) does not adequately relate this parameter to the physics of the stopping process.

ACKNOWLEDGMENTS

FOOTNOTES

[1] J. Lindhard and M. Scharff, Phys. Rev. 124, 128 (1961).

[2] G. Sauerbrey, Z. Physik, 155, 206 (1959).

[3] A technique similar to this was used by: M. Bader, R. E. Pixley, F. S. Mozer, and W. Whaling, Phys. Rev. 103, 32 (1956).

[4] J. H. Ormrod and H. E. Duckworth, Can. J. Phys. 41, 1424 (1963).

[5] H. K. Reynolds, D. N. F. Dunbar, W. A. Wenzel, and W. Whaling, Phys. Rev. 92, 732 (1953).

[6] N. Bohr, Kgl. Danske Videnskab. Selskab, Mat. - Fys. Medd. 18, No. 8 (1948).

[7] J. Lindhard and P. V. Thomsen, "Radiation Damage in Solids, Vol. I." (International Atomic Energy Agency, Vienna, 1962), pp. 65-76.

[8] A. Van Wijngaarden and H. E. Duckworth, Can. J. Phys. 40, 1749 (1962).

TABLE I. Observed stopping cross sections taken from smooth curves drawn through the experimental results.

| Energy, keV | $S_0 \times 10^{-15}$ eV cm^2 | | | |
	$He^+ - C$	$He^+ - Al$	$He^+ - Cr$	$H_1^+ - C$
66	21.7[a]	34.8	49.8[a]	15.1[a]
78	23.4	37.6	54.0	15.0
90	25.0	40.3	57.9	14.8
102	26.3	42.9	61.5	14.7
114	27.5	45.2	65.0	14.6
126	28.5	47.5	68.2	14.4
138	29.4	49.6	70.9	14.1
150	30.3	51.3	73.1	13.8
162	31.0	52.6	74.9	13.5
174	31.7	53.6	76.3	13.1
180	32.0	54.0	76.8[a]	12.9

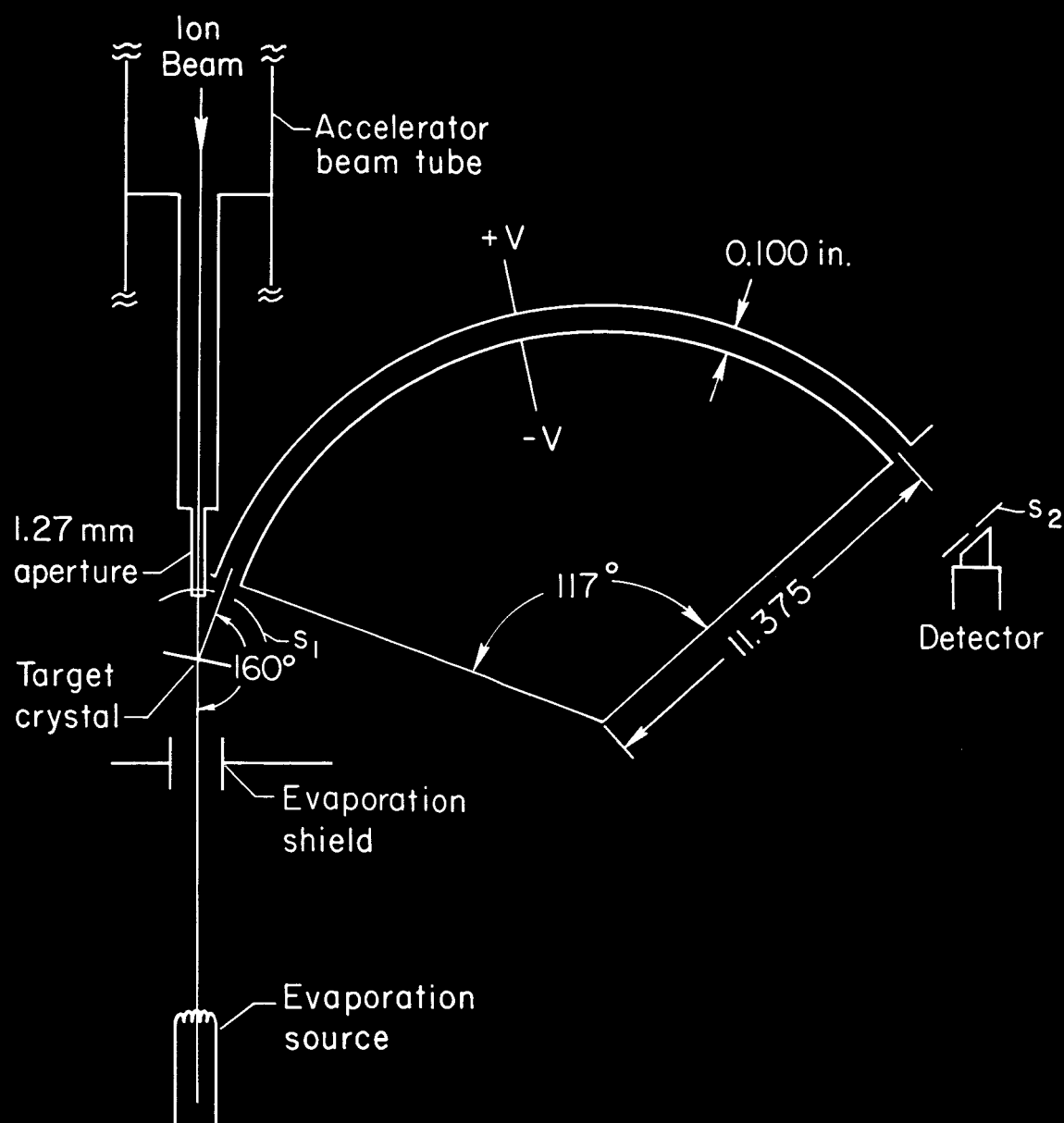[a]Values taken from curve extrapolated beyond experimental date.

FIGURE CAPTIONS

Fig. 1. Essential features of the experimental equipment.

Fig. 2. Typical energy distributions of ions scattered from the target. (Nominal energy of incident He^+ beam = 100 keV).

Fig. 3. Events degrading the energy of the ions at the target.

Fig. 4. Representative curve indicating the significance of various terms in the derivation of Eqs. (5a) and (6).

Fig. 5. Measured stopping cross section of protons through carbon.

Fig. 6. Plot comparing calculated and measured total stopping cross section, and calculated nuclear stopping cross section for He^+ through carbon.

Fig. 7. Plot comparing calculated and measured total stopping cross section, and calculated nuclear stopping cross section for He^+ through chromium.

Fig. 8. Plot comparing calculated and measured total stopping cross section, and calculated nuclear stopping cross section for He^+ through aluminum.

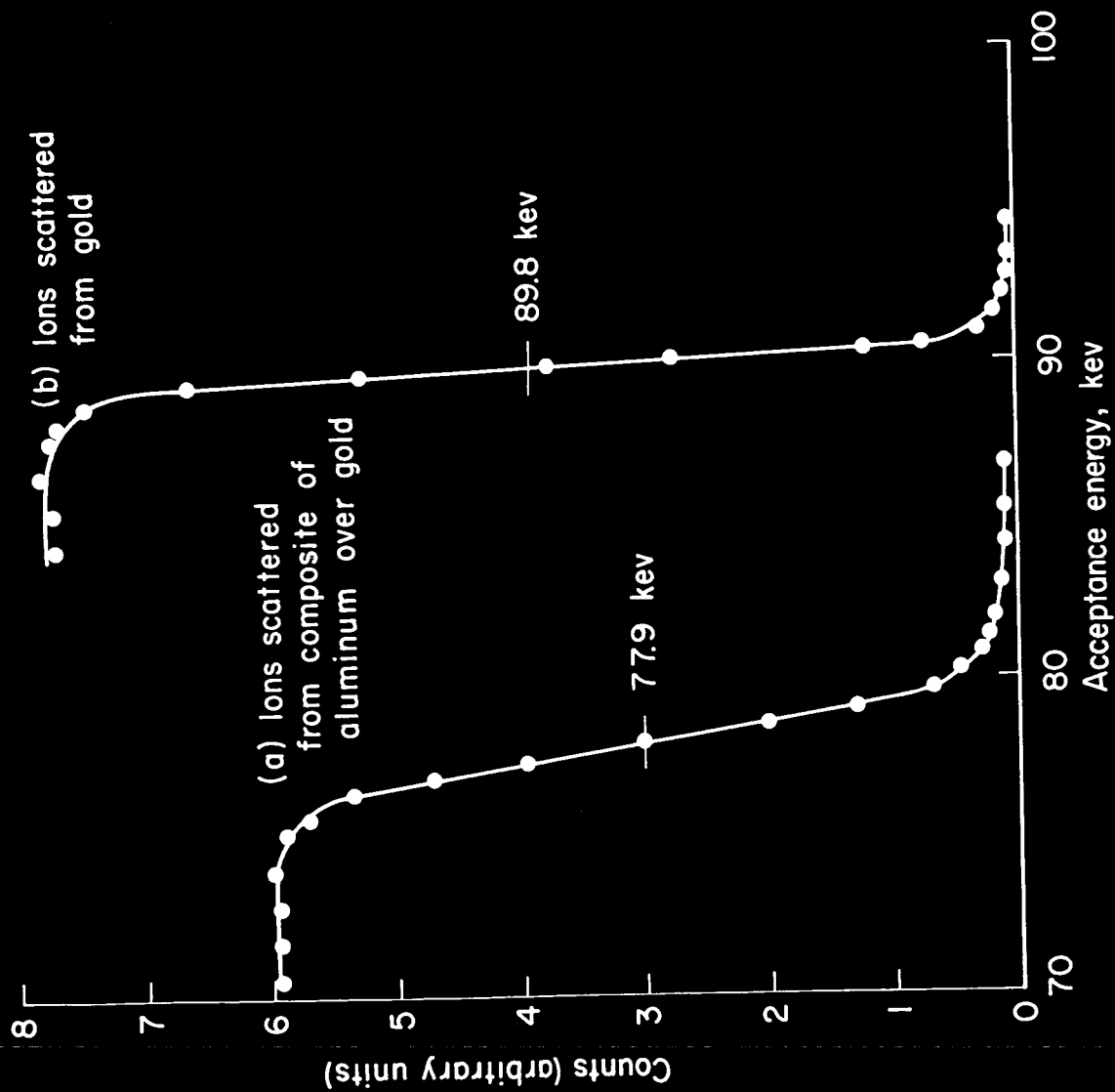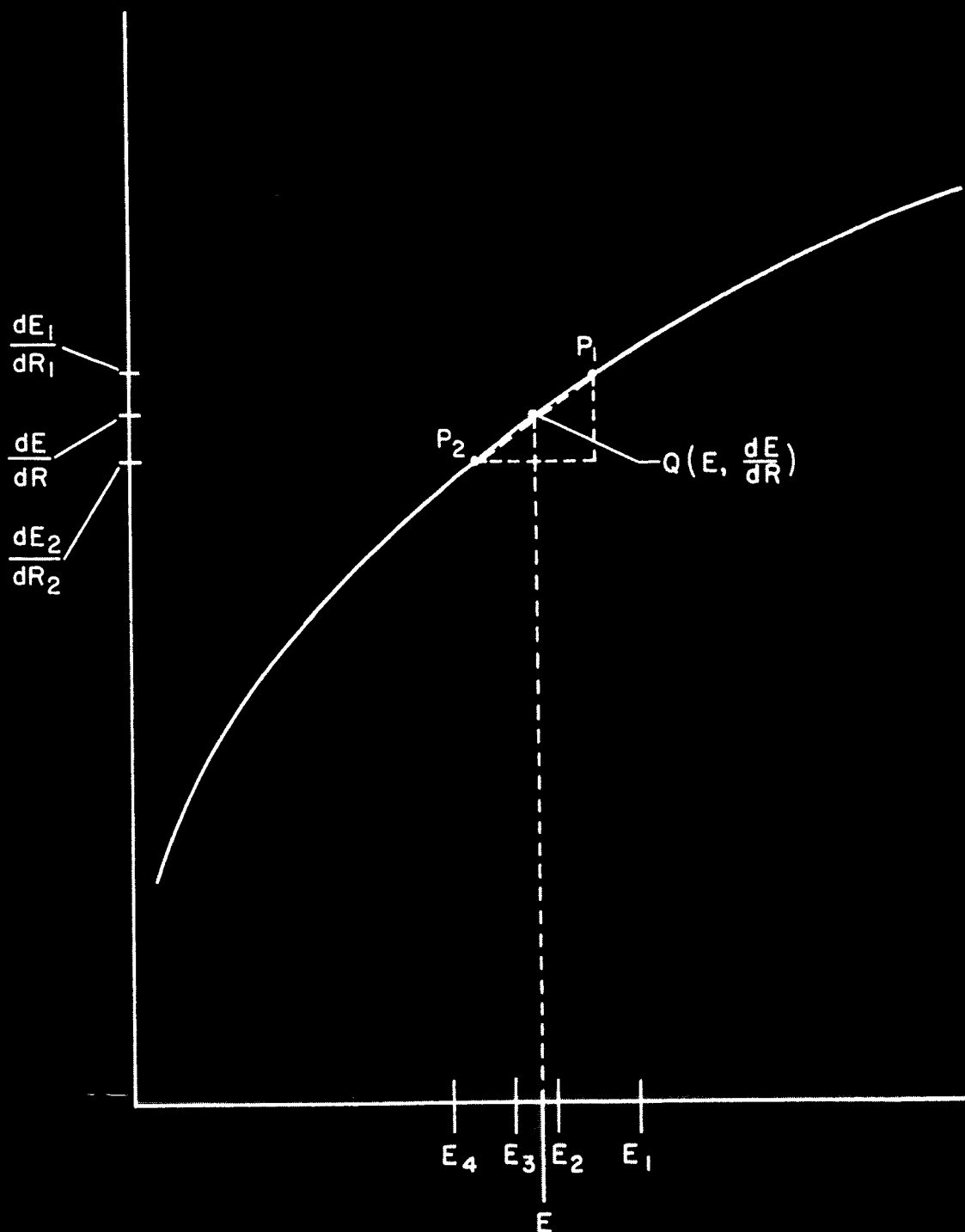Fig. 1.- Essential features of the experimental equipment.

Fig. 2.- Typical energy distributions of ions scattered from the target. (Nominal energy of incident He+ beam = 100 keV.)

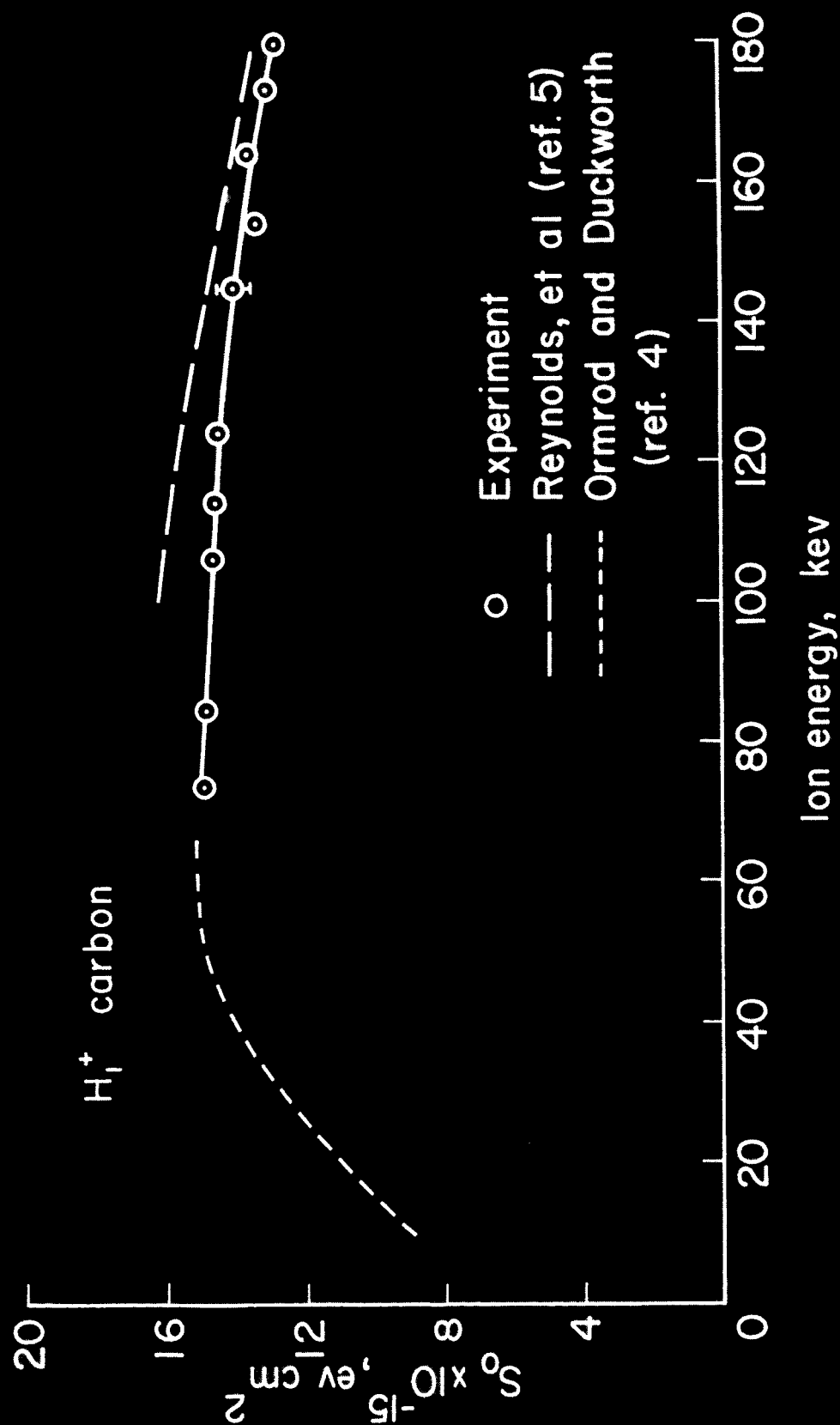Fig. 4.- Representative curve indicating the significance of various terms in the derivation of Eqs. (5a) and (6).

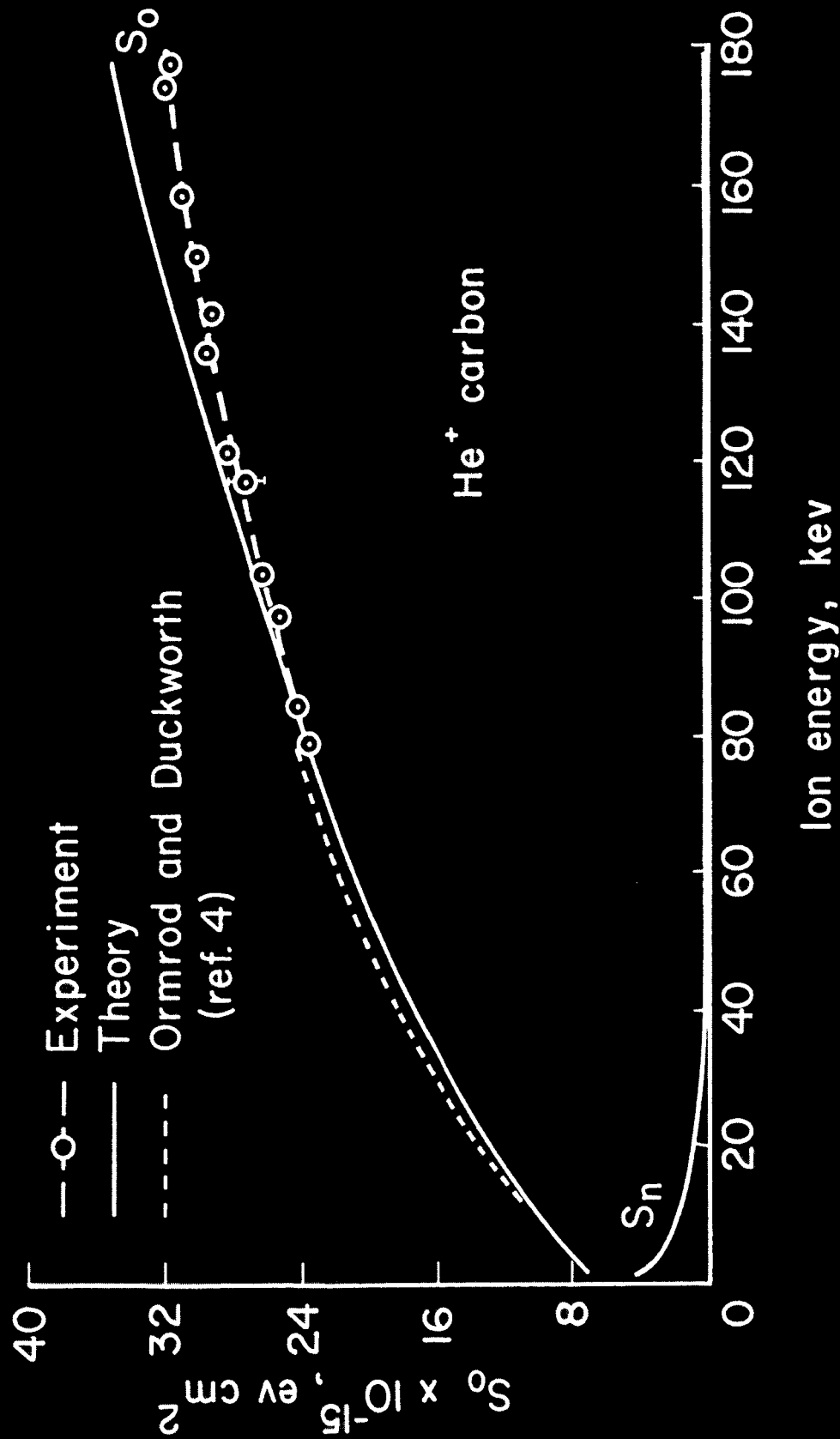Fig. 5.- Measured stopping cross section of protons through carbon.

Fig. 6.- Plot comparing calculated and measured total stopping cross section, and calculated nuclear stopping cross section for He+ through carbon.
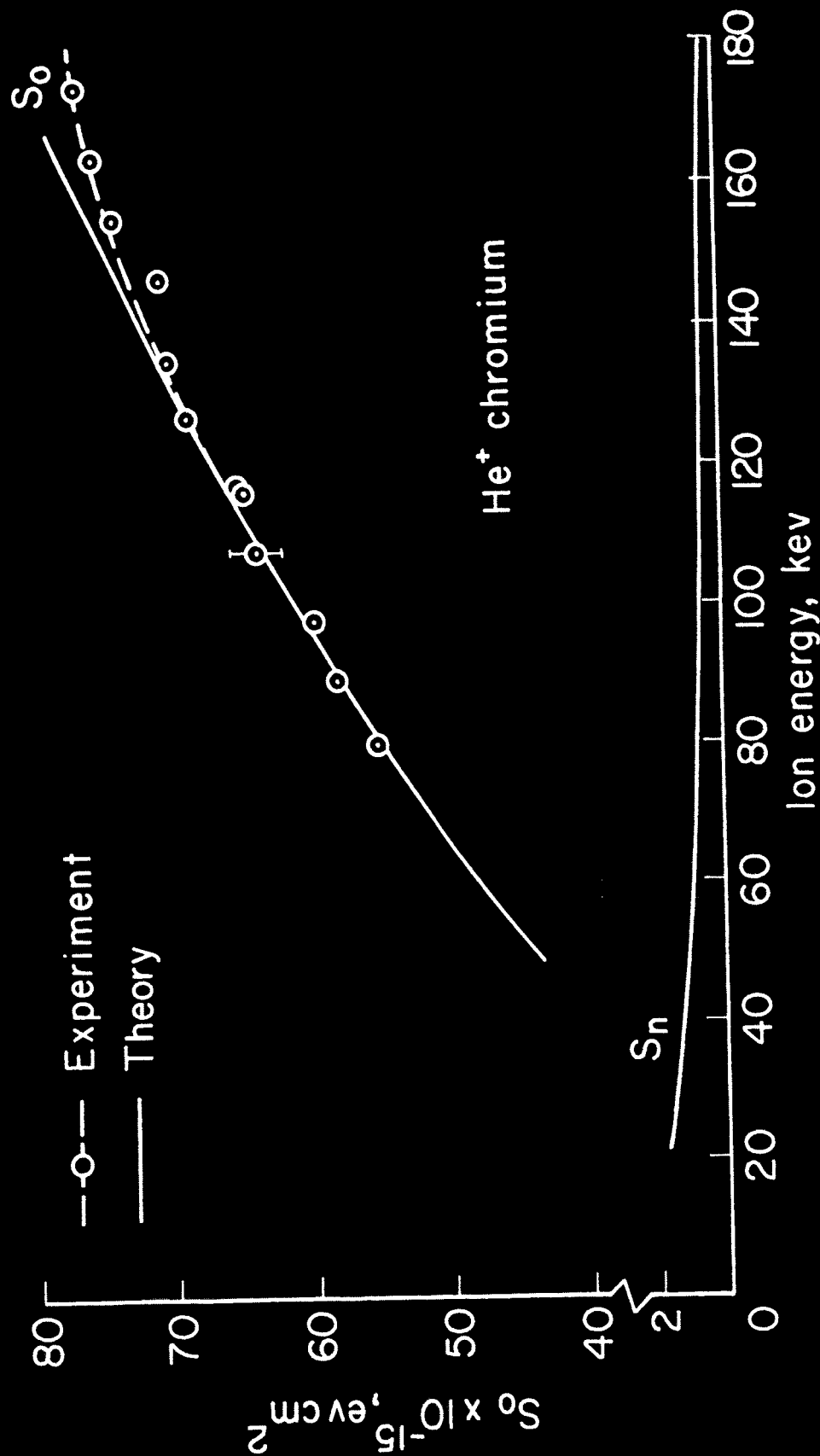
Fig. 7.- Plot comparing calculated and measured total stopping cross section, and calculated nuclear stopping cross section for He$^+$ through chromium.
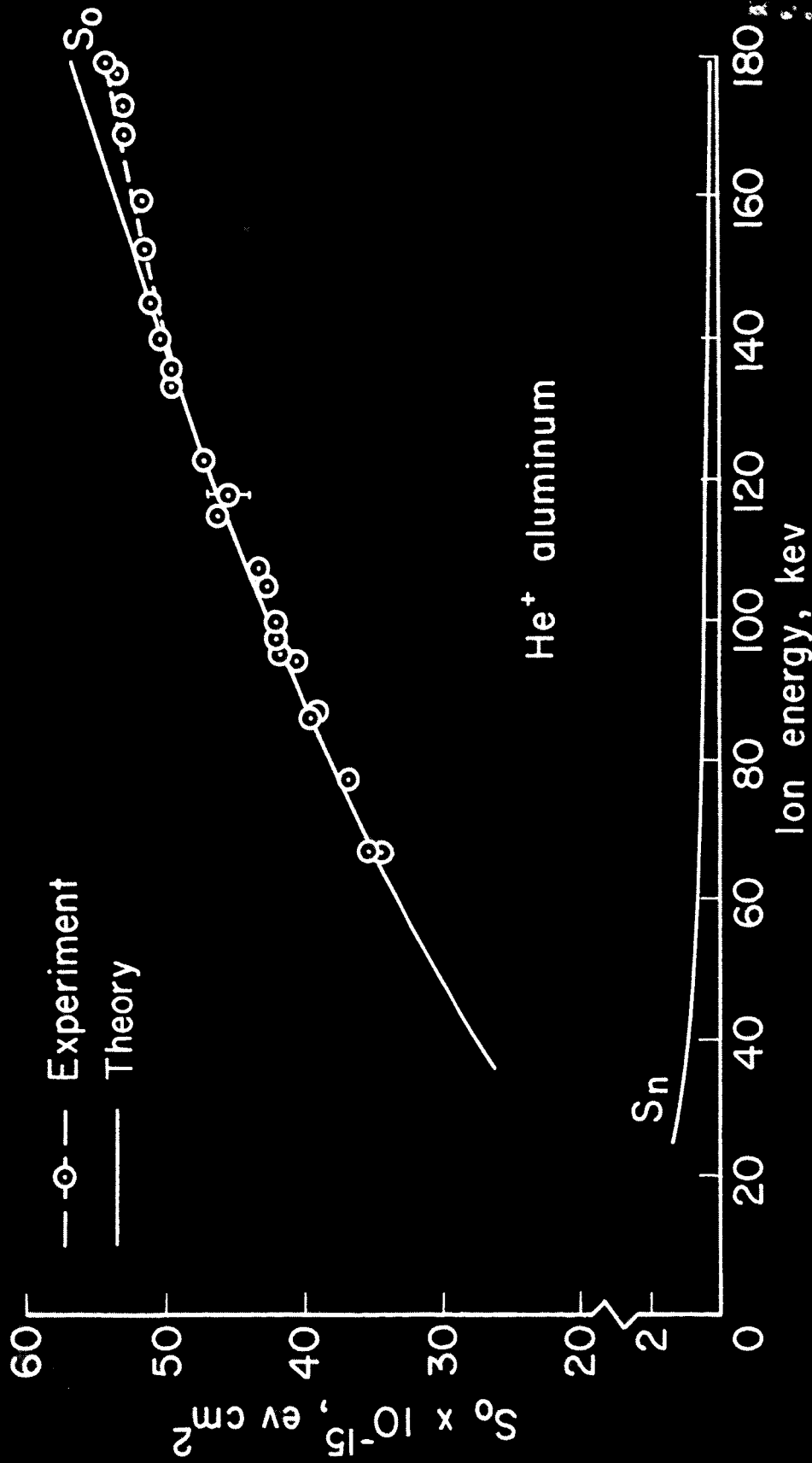
Fig. 8.- Plot comparing calculated and measured total stopping cross section, and calculated nuclear stopping cross section for He$^+$ through aluminum.